Clark Marin K. (Orcid ID: 0000-0002-6141-8422)
ANDERSON SUZANNE Prestrud (Orcid ID: 0000-0002-6796-6649)
Godt Jonathan (Orcid ID: 0000-0002-8737-2493)

Revised submission to Earth Surface Processes and Landforms XX/XX/XX

Shallow seismic profiles reveal anisotropy in critical zone architecture linked to weathering threshold

Jennifer Von Voigtlander[1,2], Marin K. Clark[1*], Dimitrios Zekkos[3], William W. Greenwood[3], Suzanne P. Anderson[4], Robert S. Anderson[5], Jonathan W. Godt[6]

[1] *Department of Earth and Environmental Sciences, University of Michigan, Ann Arbor, MI 48109, USA*
[2] now at *Schlumberger Technologies Inc., Houston, TX 77057*
[3] *Department of Civil and Environmental Engineering, University of Michigan, Ann Arbor, MI 48109, USA*
[4] *Department of Geography and INSTAAR, University of Colorado, Boulder, CO 80309, USA*
[5] *Department of Geological Sciences and INSTAAR, University of Colorado, Boulder, CO 80309, USA*
[6] *Natural Hazards Mission Area, Landslide Hazards Program, U.S. Geological Survey, Denver, CO 80225, USA*
**corresponding author*

ABSTRACT

The evolution of volcanic landscapes and their landslide potential are both dependent upon the weathering of layered volcanic rock sequences. We characterize critical zone structure using shallow seismic V_p and V_s profiles and vertical exposures of rock across a basaltic climosequence on Kohala peninsula, Hawai'i, and exploit the dramatic gradient in mean annual precipitation (MAP) across the peninsula as a proxy for weathering intensity. Seismic velocity increases rapidly with depth and the velocity-depth gradient is uniform across three sites with 500-600 mm/yr MAP, where the transition to unaltered bedrock occurs a depth of 4-10 m. In contrast, velocity increases with depth less rapidly at wetter sites, but this gradient remains constant across increasing MAP from 1000 to 3000 mm/yr and the transition to unaltered bedrock is near the maximum depth of investigation (15-25 m). In detail, the profiles of seismic velocity and of weathering at wet sites are nowhere monotonic functions of depth. The uniform average velocity gradient and the greater depths of low velocities may be explained by the averaging of velocities over intercalated highly weathered sites with less weathered layers at sites where MAP > 1000 mm/yr. Hence, the main effect of climate is not the progressive deepening of a near-surface altered layer, but rather the rapid weathering of high permeability zones within rock subjected to precipitation greater than ~ 1000 mm/yr. Although weathering suggests mechanical weakening, the nearly horizontal orientation of alternating weathered and unweathered horizons with respect to topography also plays a role in the slope stability of these heterogeneous rock masses. We speculate that where steep, rapidly evolving hillslopes exist, the sub-horizontal orientation of weak/strong horizons allows such sites to remain nearly as strong as their less weathered counterparts at drier sites, as is exemplified by the 50-60 degree slopes maintained in the amphitheater canyons on the northwest flank of the island.

Key words: critical zone, regolith formation, shallow seismic profiles, slope stability, Hawai'i, basalt weathering

INTRODUCTION

The critical zone (CZ) is defined as near-surface environments on Earth (NRC, 2001), in which life is supported, and where natural hazards that threaten human lives and infrastructure occur. Subsurface heterogeneities and environmental gradients characterizing the CZ result from complex interactions of physical, chemical, and biological processes responding to tectonic, climatic, and anthropogenic forcings over time (Brantley et al., 2007; Ritter et al., 2011; Anderson et al., 2007; Riebe et al., 2016). Our understanding of CZ structure and strength remains inadequate to incorporate in quantitative models of landscape evolution and in robust assessment of slope hazards. As such, development of future models depends on our ability to extrapolate outcrop-scale observations to geomorphically relevant scales, which in part requires understanding how individual environmental factors affect CZ evolution (Brantley et al., 2007; Anderson et al., 2007; Holbrook et al., 2013; Riebe et al., 2016).

Weathering and fracturing dramatically reduce the mechanical strength of materials in the critical zone, ultimately breaking bedrock down to transportable material (Selby, 1980; Anderson and Anderson, 2010). CZ thickness, degree of weathering and strength reduction are typically thought to be proportional to precipitation and to its residence time in the near surface (e.g. Hoek and Brown, 1980; 1997; Rahardjo et al., 2004; Brantly and White 2009; Lebedeva and Brantly, 2013; Anderson et al., 2013; Rempe and Dietrich, 2014). Hence erosion rates are associated with regional climate

(Dixon et al., 2009; Ritter et al., 2011; Murphy et al., 2016). Weathering-related weakening is often conceptually simplified as the top-down alteration of unweathered bedrock, which progressively extends rock damage to greater depths as weathering progresses (e.g., Anderson et al., 2007; Brantley and Lebedeva, 2011). However, variability in initial permeability structure, fracture density or weathering susceptibility may complicate this simple concept (e.g., Mohamed et al., 2007; Goodfellow et al., 2014). Accelerated weathering may occur in high permeability or densely fractured zones, which will produce a strength profile that differs from that resulting from simple top-down weathering into a homogeneous substrate.

The most distinct subdivision within the critical zone is that between altered and unaltered bedrock, or in engineering terms, the distinction between soil and rock. Strength values range over an order of magnitude across this continuum, which is typically observed in the upper tens of meters of the Earth's surface. The upper altered, or "damaged", layer consists of mobile regolith (i.e. material that is free to move and may be transported diffusively, often simply called soil) below which intact or immobile regolith includes a continuum from saprolite to weathered and fractured rock (Anderson et al., 2007; Anderson et al., 2013). The variability in the mechanical strength of immobile regolith is one of the least understood aspects of the near-surface rock profile (Hachinohe et al., 1999; Moon and Jayawardane, 2004; Bursztyn et al., 2015), where weathering and discontinuities of the rock mass reduce intact rock strength in rock mass classification schemes (e.g. Hoek and Brown, 1997). Because detachment of variably damaged rock from intact regolith contributes to sediment production by various means (fluvial, glacial, mass wasting), the mechanical evolution of the intact regolith should influence physical erosion rates and thus play a key role in both landscape evolution and hillslope stability.

Although the strength of weathered and fractured rock masses are described by classification schemes employed by the geotechnical engineering community (e.g., Hoek and Brown, 1980; Hoek, 1994), we lack systematic studies that integrate weathering processes with rock strength evolution. This fact limits our ability to extrapolate observed CZ structure to geologically relevant time and spatial scales. Presumably, as precipitation exerts primary control on mechanical properties of the critical zone through rock weathering, this may be quantified through spatial trends in rock strength reflected in seismic velocity profiles. As yet, interpretation of critical zone architecture from geophysical imaging is a developing science (Parsekian et al., 2015). The extreme precipitation gradient across the northern district of Kohala peninsula on the Island of Hawai’i provides an ideal natural laboratory to investigate the long-term effects of precipitation on CZ structure from P and S wave velocity profiles obtained across a uniform basalt lithology. In this study, we performed shallow seismic surveys and examined nearby vertical exposures of the rock structure. Using seismic velocity as a proxy for mechanical strength, these observations guide a conceptual model of CZ evolution as a function of MAP for Kohala. This model can be generally applied to sites in which weathering potential is stratified by either initial lithologic characteristics or subsequent fracturing. We can also relate heterogeneous weathering processes and rock strength to models of slope stability and the maintenance of unique and dramatic steep walled canyons in this setting, which challenges recent assertions of climate-modulated rock weakening as a primary control on river incision in this environment (Murphy et al., 2016).

GEOLOGIC SETTING

The Kohala Volcano is the oldest major shield volcano on the Island of Hawai'i, emerging above sea level roughly 500,000 years ago (Spengler and Garcia, 1988) (Figure 1). Pleistocene age volcanic rocks exposed in this region belong to either the older Pololu volcanics (460 to 260 ka) (McDougall, 1969; McDougall and Swanson, 1972; Spengler and Garcia, 1988) or the younger Hawi volcanics (230 to 120 ka) (McDougall, 1969; McDougall and Swanson, 1972; Wolfe and Morris, 1996; Chadwick et al., 2003). Both of these systems produced basaltic lava flows, but they differ in both structural and chemical characteristics typical of a shield building sequence. The tholeiitic Pololu volcanics are primarily pahoehoe flows, which are vesicular and have a ropey, rolling surface texture and commonly contain lava tubes. The younger, alkalic flows of the Hawi volcanics are a'a flows with a significantly rougher surface morphology and lower vesicularity compared to the Pololu volcanics (Spengler and Garcia, 1988).

Because the initial flow structure and texture likely influenced weathering and strength profiles, we restricted our data collection to locations on the Pololu volcanics. Minimal erosion of the original shield surface also makes it an ideal site in which to isolate weathering gradients as a function of precipitation.

The maximum elevation in Kohala exceeds 1600 m, producing a dramatic orographic rain shadow from southwesterly trade winds striking the northeastern flank of the volcano. The orography is reflected in an order of magnitude difference in mean annual precipitation (MAP) across the peninsula, ranging from 200 mm/year on the western side to 4000 mm/year in the east (Giambelluca et al., 2013) (Figure 1). While the precipitation gradient presumably grew as volcanic topography accumulated, and varied during glacial/interglacial periods (Chadwick et al., 2003; Porter, 2005), perceptible geographic variations in precipitation have been interpreted to exist for at least the last 50,000 years (Porter, 2005). In this study, we use variations in MAP across similarly aged basalts as a proxy for the expected weathering progression. In most cases, we were able to conduct surveys near human-made or natural exposures of the CZ from which we could evaluate both the degree of weathering and support our interpretation of the seismic velocity structure.

METHODS

Few surveys characterize variations in CZ weathering profiles across environmental gradients. Because small-scale variability in lithology, mineralogy, topography, and erosion produce heterogeneous weathering profiles, it remains a challenge to produce field data relevant to hillslope and watershed scales. Techniques such as augering and trenching are depth limited, and the expense of drilling to greater depths generally prohibits coverage over broad areas. Geophysical techniques, such as shallow seismic methods using short arrays and active sources, are ideal for hillslope scale studies because they are inexpensive and can be deployed in remote and steep topography (Parsekian et al., 2015; St. Clair et al., 2015). Shallow seismic profiling also offers advantages compared to other methods because it is non-invasive and quantification of material properties from seismic velocities has been established by the geotechnical engineering community. Two-dimensional surveys can be used to construct and constrain layer boundaries, such as the thickness of various regolith layers and the depth to unweathered bedrock, as well as to characterize horizontal variability in subsurface structure, material properties and fluid saturation (e.g., Barton, 2007, Befus et al., 2011, Greenwood et al., 2015).

Subsurface velocities are a product of material density and stiffness of intact rock, but are also very sensitive to the density of fractures, joint roughness and void spaces at a range of scales. An increase in porosity and a decrease in density and elastic moduli are associated with weathering degree and contribute to a decrease of seismic velocities as weathering progresses (Barton, 2007). The number, size and infilling of cracks, and the numbers and size of voids also affect the velocity of wave propagation through the material (e.g. Stanchits, 2006; Clarke and Burbank, 2011). Using P- and S-wave velocity as a proxy for weathering, climatic control on rock strength reduction can be quantitatively determined based on developed relationships between P- and S- wave velocities and strength, most commonly, unconfined compressive strength (UCS) (e.g. Gupta and Rao, 1998; Tugrul and Zarif, 2000; Sarno et al., 2010).

First-arrival seismic refraction studies are a common method to infer the P-wave velocity structure of the shallow subsurface depth and velocity by inferring the rate of wave propagation along various ray paths from travel-time curves (Burger et al., 2006). Tomographic methods produce two-dimensional velocity profiles from which layering and material boundaries, such as the regolith-bedrock contact, can be identified (Stokoe and Santamarina, 2000; Burger et al., 2006; Stanchits, 2006; Befus et al., 2011; Holbrook et al., 2014). Down-going seismic waves that encounter a higher velocity layer underlying a lower velocity layer are refracted along and back up toward the surface, and thus seismic refraction surveys only accurately characterize subsurface stratigraphy in which velocity increases with depth (Stokoe and Santamarina, 2000). In the opposite case, a lower velocity layer underlying a higher velocity layer would refract waves away from the surface and would not be observed, thus the inability of P-wave refraction studies to identify low-velocity layers in an alternating sequence is a limitation of the technique.

Established techniques using surface waves (i.e. Rayleigh waves) to interpret S-wave velocity profiles (a body wave) have advanced in reliability in recent years (e.g. Foti et al., 2009; Yoon and Rix, 2009; Pelekis and Athanasopoulos, 2011). These methods rely on the dispersive properties of Rayleigh waves, which refers to different wavelength (or frequency) waves traveling at different velocities, and their relationship to S-wave velocities. Where S-wave velocities change with depth, small wavelength (high frequency) waves sample shallow regions, whereas longer wavelengths (lower frequency) sample greater depths (e.g. Stokoe and Santamarina, 2000). The multichannel analysis of surface waves (MASW) method has been used to generate extensive data in a variety of natural and manmade materials (e.g. Greenwood et al., 2015; Duffy et al., 2014). MASW employs a linear array of geophones and an impulsive source, or harmonic oscillator, to generate and measure Rayleigh waves. Dispersion is characterized and then used as part of a forward-modeling inversion approach to evaluate the S-wave velocity profile (Park et al., 1998; Park et al., 1999). It should be noted that surface wave methods, in general, have difficulty identifying velocity changes in thin layers at depth because increasingly lower frequency waves are relied upon to sample greater depths, resulting in greater “averaging” of the subsurface in deeper parts of the profile (Stokoe and Santamarina, 2000). The inversion of surface wave dispersion into an S-wave velocity profile has no unique solution much like other geophysical methods (Foti et al., 2009). This means that care must be taken, or model restrictions through complementary data must be collected to ensure that a solution that is representative of the site conditions is realized during the inversion procedure.

Seismic survey parameters and processing

Seismic profiles for both P- and S-wave velocities were recorded using a 16-channel Geometrics[1] ES-3000 portable seismometer. Total survey length, as well as the velocity structure, determines the depth of investigation. Shallow profiles provided high resolution that can be compared to vertical rock sequence exposures, while deeper sections provided information about depth to unweathered bedrock. The details of each survey design and modeling parameters are reported in the Supplementary Materials.

P-wave lines were recorded with either 4.5 or 40 Hz geophones, using a sledge hammer source (2 or 8 kg) to strike a 10 cm square, 2.5 cm thick metal or 15 cm square, 5 cm thick plastic plate. Geophone spacing varied between 1 and 3 m and shots were recorded in between geophones and as off-end strikes were recorded at 1 and 5 m intervals, producing total line lengths of 15 to 45 m. This resulted in typical P-wave models with a depth of investigation of 4 to 18 m (Supplementary Materials).

We compute two-dimensional P-wave velocity profiles using a linearized tomographic inversion, suitable for sites with complicated velocity structures and lateral velocity variations. This technique can be applied to areas with less distinct velocity

[1] Any use of trade, firm, or product names is for descriptive purposes only and does not imply endorsement by the U.S. Government.

contrasts as well as to areas of layered subsurface with sharp velocity contrasts. We assume an initial linear velocity profile and apply a ray-tracing algorithm to determine the fastest theoretical travel times (i.e. the first arrival) for each receiver given specified survey geometry. The difference between the observed and theoretical travel times for the ray paths is described by the root mean square error (RMSE) and provides a means to assess the validity of the inferred velocity models. Choice of initial velocity model on the resulting theoretical travel time curve has a small effect on the final velocity model, the variability of which we estimate to be 40 m/s (1-standard deviation) (Supplementary Materials). Theoretical travel time curves are generated from the initial velocity model and then iteratively changed in order to find a best fit between theoretical and observed travel times. Seisimager software module Pickwin and Plotrefa were used to produce time travel curves and to invert the waveform interpretation for a velocity structure of the shallow subsurface respectively (OYO Corporation, 2006; Hayashi and Takahasi, 2011).

Seismic profiles for S-wave velocity were measured using, initially, the same survey lines as the P-wave profiles, then were shifted by one sensor spacing (1 to 3 m) in the direction of the array in order to produce a 2D array (Supplementary Materials). Rayleigh waves were measured using 4.5 Hz geophones spaced at 1 to 3 m and impulsive sources were generated using a 2 to 8 kg hammer on a 15 cm square, 5 cm thick plastic plate (Supplementary Materials). The source was input at an offset of about

15-20% of the total array length to avoid near-field effects (Yoon and Rix, 2009). Shots were stacked 5-10 times to improve signal-to-noise ratio.

Surface wave measurements were processed using the common mid-point cross-correlation (CMPCC) procedure (Hayashi and Suzuki, 2004). CMPCC is an extension of the traditional one-dimensional and two-dimensional MASW procedures (Park et al., 1998; Xia et al., 2000) and is intended to improve spatial resolution in the final profile (Hayashi and Suzuki, 2004). Both fundamental and higher-mode Rayleigh waves were considered in the analysis. Higher-mode Rayleigh waves arise in specific subsurface conditions, such as low-velocity layers interbedded with high-velocity layers (Stokoe et al., 1994). Utilizing higher-modes in these site conditions is necessary to improve resolution and depth of investigation, stabilize inversion results, and realize complex subsurface velocity structures (Xia et al., 2003). An initial velocity structure was assumed and the dispersion curves were back-calculated and compared with the measured dispersion curves. The S-wave velocity profile was then iteratively adjusted until the best dispersion curve match was achieved. This is often done using a least squares method. The best dispersion curve matches were used to generate the final S-wave velocity profiles.

SEISMIC VELOCITY PROFILES

The comparison of velocity profiles as a function of mean annual precipitation is used to interpret changes in critical zone architecture as a function of weathering, assuming precipitation as a proxy for weathering degree. P-wave velocity cross-sections derived from the linearized tomographic inversion are presented for eight study sites. In addition, S-wave profiles from three of the eight sites accompany the P-wave data. Results are summarized in two groups: dry sites (500-600 mm/yr MAP) and wet sites (> 1000 mm/yr MAP). At most sites, vertical exposures of 4-10 m height in the vicinity of the seismic survey are used to compare velocity measurements to rock fracture patterns and field observations of weathering degree.

Dry sites (500-600 mm/yr MAP)

Surveys were conducted at three sites on the dry (leeward) side of the Kohala peninsula with similar MAP (500-600 mm/yr) (Figures 1 and 2). Variable geophone spacing for overlapping profiles produced both high resolution in the near surface (4 meters depth) as well as greater depth of investigation (18 m maximum) at lower resolution.

P-wave data obtained using 1.0 m and 1.5 m spaced lines generally show steep velocity gradients in the upper few meters of the section, below which velocities are constant or increase more gradually with increasing depth (Figure 2). The slowest velocity layer (300-500 m/s) is 0-2 meters thick and is underlain by velocities of 500-1500 m/s extending to 3-4 meters depth. Modeled V_p velocities are laterally discontinuous nearest the surface, consistent with the patchy exposure of corestones interspersed with saprolite and sandy soil. Greater line spacing (2.5 – 3 m) results in models with a more gradual increase in velocity over this same depth and velocity interval compared to the 1 and 1.5 m spaced lines. This likely occurs because V_p velocities are averaged or smoothed out and these models have higher modeled misfits to the data as a result of the wider geophone spacing (Figure 2, Supplementary Data). At the sites with the greatest depth of investigation (18 m), maximum velocities reach 3500 m/s to 3800 m/s at 7 – 15 meters depth.

A single S-wave profile for the dry sites shows similarly steep V_s velocity-depth gradients as the P-wave data (Figure 2). Within the upper three meters, the lowest S-wave velocity is 200-300 m/s. However, this near surface lower V_s velocity layer is laterally discontinuous and reaches higher velocities of 500 m/s toward the north end of the line. Like the P-wave data, along-strike variability in the near surface V_s velocities is consistent with surface exposures of both rock and soil. Near the maximum depth of investigation (12 m) V_s velocities reach 650-700 m/s.

Wet sites (> 1000 mm/yr MAP)

Four P-wave surveys were collected at sites with variable MAP on the wet, windward side of the island (MAP ~ 1000-3000 mm/yr) (Figures 1 and 3), and two S wave profiles were collected at sites with 1000 (Airport) and 1500 (Lighthouse) mm/yr

MAP (Figure 4). As with the dry sites, variable geophone spacing for individual profiles produced higher resolution in the near surface with closer geophone spacing (4 meters depth) as well as greater depth of investigation using larger geophone spacings (25 m maximum depth). Two of the surveys were collected at coastal sites adjacent to sea cliff exposures (Airport and Lighthouse). Two other surveys were collected within the steep amphitheater canyons on the northeast side of the peninsula (Awini landslide and Waipio Canyon).

Similar to the dry sites, the P-wave surface layer of the wet sites is associated with steeper velocity/depth gradients in survey lines with 1 and 1.5 m spacing compared to larger spacings. However, the surface V_p velocity layer (300-500 m/s) is thicker (5-10 m compared to 0-2 m for the dry sites, with the exception of the Awini landslide) (Figure 3). Below this surface layer, V_p velocity increases with depth more gradually compared to the dry sites. Maximum V_p velocities reach 1200 m/s to 1500 m/s at the maximum depth of investigation (12-15 m depth) and are much lower than the velocities at equivalent depths at dry sites. The exception is the Awini landslide site where the profile was collected across a landslide scar. Here, the surface layer (V_p = 300-500 m/s) is thin to non-existent and V_p velocities below this horizon (800-1200 m/s) at depths of up to 3 meters are higher than at equivalent depths on the other three wet sites. Presumably the landslide removed a lower V_p velocity surface layer.

S-wave profiles show stratification with prominent high and low velocity horizons that are laterally discontinuous (Figure 4). At the Airport site (MAP ~1000 mm/yr), the upper seismic stratum displays V_s velocities as low as 100-200 m/s in a discontinuous layer ~ 2 m thick. This surface horizon is underlain by a zone of fast V_s seismic velocities (400-600 m/s) extending down to 4 meters depth. A prominent subsurface low-velocity horizon (V_s = 100-200 m/s) is modeled between 4-8 m depth. Similarly, the Lighthouse profile (MAP ~ 1500 mm/yr) shows stratification with a low velocity surface horizon underlain at depth with discontinuous high velocity horizons at 3-7 m depth, and low velocity horizons between 5 and 10 meters depth. In both profiles, V_s velocities increase at greater depths (> 10 m) to 450 m/s at 14 meters depth to more than 550-600 m/s at the maximum depth of investigation (25 m). The alteration of low to high V_s velocity in the upper 10 meters of the profile corresponds to intervals of greater/lesser weathering in sea cliff exposures adjacent to the profiles (Figure 4).

SEISMIC CHARACTERIZATION OF THE CRITICAL ZONE

Rock weathering at the dry site Road Cut East (Figure 2), previously described by Goodfellow et al. (2014), provides a weathering classification scheme for the seismic velocity model. The classification scheme extracted from this comparison was used at the other dry sites (MAP 500-600 mm/yr), but cannot account for the observed layering of material properties observed for wet sites (MAP > 1000 mm/yr). Presumably, the presence of soft, weathered material lowers the seismic velocities, resulting in a different characterization of the critical zone for wet sites and is readily observed as low velocity horizons on S-wave profiles (Figure 4).

Dry sites (MAP 500-600 mm/yr)

We superimpose the geochemical weathering profile characterized by Goodfellow et al. (2014) on the Road Cut East 1m V_p profile (Figure 5). There is a good correspondence between the uppermost velocity layer (V_p = 300-500 m/s) and a layer identified as “soil (clast-rich)” (all weathering descriptions in quotations are those of Goodfellow et al. (2014) and were determined based on chemical depletion measured from samples as well as outcrop characteristics). The next lower layer is a mixture of “saprolite” and “slightly weathered rock”, where we observe V_p = 500 – 1500 m/s. Below 2 m depth, the outcrop is characterized mainly as fractured, “unweathered rock” and corresponds to P-wave velocities of 1500 – 2000 m/s and V_s = 500 m/s. This “unweathered” distinction by Goodfellow et al., (2014) is made on the basis of chemical alteration, and we note that this layer contains rock that is intensely fractured and commonly has a vesicular texture, and thus is physically weathered.

We collected Silver Schmidt Hammer measurements on the outcrop as well, and found that measurable rebound values could only be obtained on rocks classified by Goodfellow as “slightly weathered rock” and “unweathered rock” in the road cut, as well as on corestones exposed at the surface along the seismic profile. The softer material of the saprolite and soil result in null rebound values. Silver Schmidt rebound measurements, or “Q-values”, vary from a mean of 24.1 $\pm$ 9.1 for “slightly weathered rock” to 30.9 $\pm$ 7.2 for “unweathered rock”, which is consistent with a lower velocity for layers classified by Goodfellow as “slightly weathered rock” compared to “unweathered rock”. Slightly weathered to unweathered blocks make up a larger proportion of each layer of increasing seismic velocity, which further suggests that the seismic velocity reflects the average properties of a layer. We also note that Silver Schmidt Hammer rebound values tend to increase downward, similar to the observed increase in V_p seismic velocity. At greater depth (i.e. below the exposure in the road cut), we observe an increase in velocity to a maximum V_p = 3000 m/s at 12 m depth (Figure 2, Road Cut West 3-m spacing line). At these same depths, V_s increases to 700 m/s.

While these observed maximum seismic velocities (V_p = 3000 m/s and V_s = 700 m/s) are lower than typically reported for basalt (V_p = 5400-6400 m/s and V_s = 2700-3200 m/s) (Barton, 2007), we suggest that vesicularity and fracturing present in the young basalts we measured, as well as the low confining stress present in near surface conditions, yield lower maximum V_p velocities for this study site compared to other critical zone investigations (Befus et al., 2011; Holbrook et al., 2014; Parsekian et al., 2015). Three lines of evidence lead us to interpret the maximum seismic velocities in Kohala as representing chemically unaltered, but fractured or vesicular rock at depth. First, our maximum V_s velocities are equivalent to previously reported “unweathered basalt" S-wave velocities for the Kohala peninsula (670 m/s, Wong et al., 2011) based on a greater depth of investigation (up to 70 m depth) than presented in this study. The relative consistency of V_p and V_s as a function of depth for a constant V_p/V_s ratio, suggests that V_p and V_s are well correlated in this environment (Figure 6) and gives us confidence in extrapolating the V_s interpretation to the V_p profiles. Second, in top flow basalts, vesicles formed during magma degassing generate pore space, and micro-/macro- cracks are generated during cooling, but these features diminish as the rock is subsequently buried to greater depths. Vesicles and cracks have been shown to dramatically reduce seismic velocities compared to massive basalts. For example, Al-Harthi et al. (1999) demonstrated an exponential decrease in V_p over the range from 2 – 6.5 km/s as a function of porosity for basalt cores from Saudi Arabia (at zero confining pressure). Cerney and Carlson (1999) measured a range in V_p for basalt cores IDP Hole 990A on the southeast Greenland margin during Ocean Drilling Program Leg 163, from 2.2 – 6.5 km/s, reflecting differences in down-hole rock properties, mainly mineralogy and porosity (~ 2 – 7 % porosity). Third, we measured 1-D P-wave profiles on a historic flow with pahoehoe textures in order to evaluate the initial V_p velocity of the Pololu volcanics just following crystallization and prior to any further weathering at the Earth's surface. Observed velocities were even slower despite the absence of chemical weathering (300 – 1000 m/s (Supplementary Materials)).

As a result, we classify P-wave velocity through critical zone material at dry sites as follows: soil (<500 m/s), saprolite/ slightly weathered rock (500 – 1500 m/s), and chemically unaltered, fractured basalt (> 1500 m/s) reaching a maximum of 3000 m/s (Figures 2 and 5). Similarly, soil V_s velocities range from as low as 100-200 m/s, increase to 200-500 m/s for saprolite/weathered rock, and reach values of unaltered basalt at >500 m/s. The soil layer is interpreted to range from 0-2 m thick, consistent with the surface exposure of corestones and rock along surveyed profiles where the soil layer is absent. The thickness of the saprolite/weathered layer averages 2-4 m. We interpret unaltered basalt at depths of 2-4 meters for the road cut sites, 5-6 m depth at Sapphire Cove and 2-4 m at Kapa'a Beach. It is an important point that the Kohala critical zone is mechanically "pre-weathered" in its initial state by processes associated with magma degassing and cooling due to vesicles and fractures. Thus we relate the changes in velocity for chemically unaltered rock, from 1500 – 3000 m/s, to likely be related to closing of vesicular pore space and cracks, which are present in near surface flow layers.

Wet sites (MAP > 1000 mm/yr)

For wet sites, we observe interbedded horizons of stiff and soft material below the surface soil horizon. Where sea cliffs are present along studied profiles, this interbedding is present down to the base of the cliff, which correlates with a stiff, resistant layer. In outcrop, the layers commonly contain variably weathered fractured bedrock or corestones; some horizons are quite intact with only incipient weathering on fracture or joint surfaces. Although V_p and V_s seismic velocities were lower at the surface in the wet sites than the dry sites, outcrops reveal weathered rock and corestones present throughout the profile. Thus, the classification scheme derived from Goodfellow et al. (2014) that we employed for the dry sites was not directly applicable to velocity models obtained on the wet sites. Instead, we suggest that the observed soft layers in the subsurface lower the average V_p and V_s velocity for a given model horizon (Figure 4). This relationship is observed at the Airport and Lighthouse site, where S-wave velocity data resolves a 1 to 4 m thick low-velocity horizon at 3 and 7 meter depths. We note that the thickness and velocity of the low-velocity horizon are not uniquely constrained. For example, the dispersion data could also match a model with a thicker low-velocity layer of somewhat higher velocity. At the Airport site, the low V_s velocity layer corresponds with the outcrop of a reddish, soft saprolite horizon interpreted to have soil-like material properties, which underlies a more resistant layer of fractured bedrock and abundant corestones. The overall effect of this layered structure is to lower the *average* P-wave and S-wave velocity over a larger depth interval.

For wet sites, the interpreted near-surface soil thicknesses were similar to dry sites (1-2 meters generally, although less than 1 meter at the Awini landslide site) (Figures 4 and 5). However, the average V_p and V_s velocity of this layer is lower than on the dry sites (Figure 6), which may be due to higher clay content associated with more pronounced chemical mineral alteration. Below the soil, we interpret a zone of interbedded slightly weathered basalt and saprolite with more deeply weathered layers. This interval typically extends to depths of 15 – 25 meters depth, which is the maximum depth of investigation for our profiles. These depths correspond to P-wave velocities of 1200-1700 m/s and S-wave velocities of 500-700 m/s, which overlaps with the lowest velocities that we associate with unaltered basalt at dry sites and with the S-wave velocities of “unweathered basalt” reported by Wong et al., 2011 (670 m/s), but do not reach the maximum velocities that we observe on the dry sites.

Throughout Kohala, the groundwater table lies at or within a few meters of sea level (Oki et al., 1999). Thus, groundwater may influence the P-wave velocity for some of our sites collected near sea level (Sapphire Cove, Kapa’a Beach, Upolo Airport and the Lighthouse). Based on studies of analogous rocks, water saturation could perturb the V_p velocities by several hundred meters per second. For example, a study of vesicular basalts from the western Snake River Plain reproduced bulk modulus predictions from physical models for fluid substitution in porous rocks (Gassmann’s relation) for frequencies less than 20 Hz (Adam and Otheim, 2013), and suggest a 500 m/s increase in V_p at low confining pressures (~3 MPa) for water-saturated basalts with 10-20% porosity. Weathering can also influence fluid substitution through the introduction of clay, and could produce both increasing and decreasing trends in V_p (up to +/- 400 m/s) for increasing degrees of saturation depending on the lithology, pore space, and clay concentration (Karakul and Ulusay, 2013).

However, two lines of evidence give us confidence in our assertion that the water table for sites near sea level did not significantly influence our interpretations. First, we do not see a systematic changes in V_p at sea level (the estimated groundwater level) for sites near the coast compared to those at higher altitudes (Figure 6). Second, the groundwater table does not affect V_s and we observe similar average gradients for V_p and V_s for dry and wet sites respectively and a constant V_p/V_s ratio, suggesting that the V_p profiles are not perturbed by the water table (Figure 6).

DISCUSSION

Precipitation, as a proxy for chemical weathering, appears to influence the depth and structure of the critical zone across the Kohala peninsula. Dry sites have thin regolith (less than 4 m), with shallow depth-to-unaltered bedrock. Where observed, the interpreted depth to unaltered, fractured and vesicular bedrock (V_p >1500 m/s and V_s> 500 m/s seismic velocities) occurs at depths of between 2 and 6 meters. By comparison, wet sites have thicker, highly-weathered regolith and do not reach the same maximum velocities as dry sites at a depth of investigation 18 m for P-wave profiles and 25 m for S-wave profiles. Because the highest interpreted velocities at the maximum depth of investigation were lower than the maximum unaltered bedrock values on the dry sites, we speculate that weathered horizons are interbedded with less weathered horizons (or even unweathered) to at least 25 m depth.

Dry sites and wet sites have distinct velocity-depth gradients (Figure 6). These gradients are bimodal, clustering around one value for dry sites (MAP ~ 500 – 600 mm/yr) and decreasing more than three-fold to another value for sites wet sites (MAP ~ 1000 - 3000 mm/yr) with a V_p/V_s ratio of 3.2. The velocity-depth gradients do not systematically decrease with increasing precipitation among wet sites. One possible explanation is that the initial permeability structure of the basalt flow sequence dictates the weathering susceptibility in the upper tens of meters of the shield surface (Oki et al., 1999; Goodfellow et al., 2014). Chemical weathering rates in Hawai'i are observed to be non-linear, where above a precipitation threshold weathering rates increase dramatically compared with drier sites but do not increase further with increasing rainfall (Porder et al., 2007). We speculate that where MAP exceeds 1000 mm/yr in this particular environment, a weathering threshold is reached above which high-permeability basalt horizons undergo rapid weathering and reach soil-like material properties, and contrast with other less permeable layers that weather only slightly and retain rock-like material properties. We hypothesize that the absence of further reduction in the velocity gradient with yet greater precipitation reflects a threshold beyond which further weathering (and associated softening/weakening) of high-permeability zones to soil-like properties cannot occur (i.e., the rock has weathered to residual soil) and that weathering of low-permeability zones are insensitive to the differences in precipitation observed here. This suggests that the governing factor on the reduction of seismic velocity at the wet sites is the rapid weathering of high permeability horizons within a layered sequence.

An interbedded weathering profile in which highly weathered and nearly unweathered layers are intercalated provides an alternative to a simple top-down weathering model, and provides insight into the weathering process and its effects on the near surface strength profile (Figure 7). While interbedding of stiff and soft materials lowers the average P-and S- wave velocities as evaluated by surface-based methods, the average strength of the near surface profile and its effect on slope stability likely depends on both the ratio of end-member materials and the orientation of layers with respect to hillslope aspect. Generally, the introduction of weak layers within a heterogeneous rock mass results in a back-calculated lower strength for landslides within the rock mass, when the geometry (orientation, thickness, and depth) of the weak layer dominates the shear resistance of the landslide mass (e.g., Duffault, 1981; Marinos and Hoek, 2001; Marinos, 2010). However, the average strength is likely dependent on the ratio of intact strength of the end member materials (Tziallas et al., 2013; Mohamed et al., 2008) and the disturbance/orientation of the layering (Marinos, 2010). At our sites, the nearly horizontal layering of stiff, slightly weathered to unweathered basalts within the Pololu flows on Kohala has the following effects: (a) To restrict failure surfaces (landslides) to shallow depths in the more weathered layers only; and (b) for deeper failure surfaces that intersect both the unweathered and weathered layers, a back-calculated, or estimated strength based on an observed slope failure, would yield a higher average strength than would be estimated without such layering (Figure 7). Within sedimentary rock sequences, sub-horizontal layering of strong and softer layers produces smaller critical failure surfaces than would have been otherwise expected for uniform rock mass properties using theoretical predictions of slope failures (e.g. Zekkos et al. (2008)).

The steep walls of dramatic canyons provide insight to the hillslope-scale rock strength properties of the wet side of Kohala. These steep-sided, amphitheater canyons common to the windward facing slopes (e.g., Lamb et al., 2007) are among the most striking features of the Hawaiian Islands. Here the 60° and steeper hillslopes that define the amphitheater heads and walls of the canyons persist despite precipitation rates of over 4000 mm/yr. We speculate that the high hillslope-scale rockmass strength implied by these steep hillslopes reflects two attributes of the setting: the interbedding of highly weathered intervals with largely unweathered layers that remain stiff and strong, and the sub-horizontal dip of the bedding, which is therefore nearly orthogonal to the steeply inclined hillslopes. As such, the link between precipitation and weathering of heterogeneous rock profiles and its relationship to various geomorphic processes, including landsliding, is a potential avenue for future investigation.

While the influence of physical erosion rate on chemical weathering is well recognized (e.g., West et al., 2005; Ferrier and Kirchner, 2008; Dixon et al., 2012; Larsen et al., 2014), the role of chemical weathering on the strength profile of a rock sequence potentially influences the nature and rate of physical erosion processes (e.g., Molnar et al., 2007; Sarno et al., 2010; Han et al., 2014). The Kohala peninsula in Hawai'i is an extreme example of what is likely a common weathering-strength phenomenon. In any heterogeneous rock mass in which spatial variation in material properties such as permeability and weathering potential exist, pronounced layering at the scale of the hillslopes can produce heterogeneous weathering profiles and anisotropic mechanical properties. For instance, the most productive aquifers in Hawaii are found in sequences with permeable layers between lava flows that direct water flow (Oki et al., 1999). Sedimentary sequences, metamorphic terrains and highly tectonized environments where rock fracturing may influence the weathering potential are likely to display similar weathering trajectories. Because the structure of the subsurface dictates the mechanical behavior, especially in weathered and weak rock masses (Hoek and Brown, 1997; Marinos and Hoek, 2001; Marinos, 2010), the presence of weak horizons and their orientation relative to the topographic surface must be taken into account when estimating bulk rock strength relevant to both the study of landscape evolution and the assessment of geologic hazards. The generation of strong regional anisotropy and non-monotonic depth profiles of weathering in some geologic settings contrasts with a simple top-down weathering-related strength profile and may invalidate simple correlations between precipitation, chemical weathering and rock strength at scales relevant to physical erosion processes (e.g., Murphy et al., 2016).

CONCLUSIONS

We hypothesize that the stratified permeability structure of the Kohala basalt sequence has produced a hillslope-scale anisotropic rock mass strength profile. Low-seismic velocity horizons correspond to exposures of soil-like material and deeply weathered saprolite. The presence of interbedded, highly weathered horizons to depths of tens of meters may explain the decrease in P- and S- wave velocity-depth gradients for sites >1000 mm/yr MAP and the uniformity of these profiles with increasing precipitation. A model of rock strength that is derived from intercalated weak and strong layers differs fundamentally from that expected from simple top-down propagation of a weathering front, which otherwise would be predicted to progressively weaken hillslopes with increasing precipitation. Instead, under circumstances in which the layering is orthogonal to hillslopes, hillslope-scale strength anisotropy might maintain rather than reduce hillslope stability. These results emphasize the need to understand weathering-related evolution of the full rock-strength profile, acknowledging that anisotropy can also influence properties of the hillslope-scale rock mass and may be an important feature of critical zone architecture in many geologic settings.

ACKNOWLEDGMENTS

This work was supported by a collaborative award from the USGS National Earthquake Hazards Reduction Program (NEHRP) grants G15AP00007 and G15AP00008 to M. Clark, R. Anderson and S. Anderson, Rackham Graduate Student travel grants (University of Michigan), the Scott Turner fund (Dept. of Earth and Environmental Sciences, University of Michigan), discretionary funding from the University of Michigan, a CIRES Visiting Faculty Fellowship from CU Boulder to M. Clark and partial funding from the National Science Foundation (NSF), Division of Civil and Mechanical Systems under Grant No. CMMI-1362975, and NSF EAR-1331828 to S. Anderson. Any opinions, findings, conclusions and recommendations expressed in this paper are those of the authors, including the views of the U.S. Geological Survey, but do not necessarily reflect the views of the other funding agencies. We thank Katherine Lowe and Mitsuhito Hirose for field assistance during the seismic data acquisition and Lou Derry for logistical guidance.

Clark Marin K. (Orcid ID: 0000-0002-6141-8422)
ANDERSON SUZANNE Prestrud (Orcid ID: 0000-0002-6796-6649)
Godt Jonathan (Orcid ID: 0000-0002-8737-2493)

REFERENCES

Adam L, Otheim T, 2013. Elastic laboratory measurements and modeling of saturated basalts. J. Geophys. Res Solid Earth 118: 1–12. doi:10.1002/jgrb.50090.

Al-Harthi AA, Al-Amri RM, Shehata WM, 1999. The porosity and engineering properties of vesicular basalt in Saudi Arabia. Engineering Geology 54(3): 313-320. doi: 10.1016/S0013-7952(99)00050-2.

Anderson RS, Anderson SP 2010. Geomorphology: the mechanics and chemistry of landscapes. Cambridge University Press; 2010 Jun 17.

Anderson RS, Anderson SP, Tucker GE 2013. Rock damage and regolith transport by frost: an example of climate modulation of the geomorphology of the critical zone. Earth Surface Processes and Landforms 38: 299–316. doi: 10.1002/esp.3330.

Anderson SP, von Blanckenburg F, White AF 2007. Physical and chemical controls on the critical zone. Elements 3: 315-319.

Barton N 2007. Rock quality, seismic velocity, attenuation and anisotropy. CRC press.

Befus KM, Sheehan AF, Leopold M, Anderson SP, Anderson RS 2011. Seismic constraints on critical zone architecture, Boulder Creek Watershed, Colorado. Vadose Zone Processes 10(3): 915-927. DOI:10.2136/vzj2010.0108.

Brantley SL, Goldhaber MB, Ragnarsdottir KV 2007. Crossing disciplines and scales to understand the critical zone. Elements *3*(5): 307-314.

Brantley SL, White AF 2009. Approaches to modeling weathered regolith. Reviews in Mineralogy and Geochemistry 70(1): 435-84. doi:10.2138/rmg.2009.70.10.

Brantley SL, Lebedeva M 2011. Learning to read the chemistry of regolith to understand the critical zone. Annu. Rev. Earth Planet. Sci 39; 387-416. doi: 10.1146/annurev-earth 040809-152321.

Burger HR, Sheehan AF, Jones CH 2006. Introduction to Applied Geophysics: Exploring the Shallow Subsurface. WW Norton.

Bursztyn N, Pederson JL, Tressler C, Mackley, RD, Mitchell KJ 2015. Rock strength along a fluvial transect of the Colorado Plateau- quantifying a fundamental control on geomorphology. Earth Planet. Sci. Lett 429; 90-100. doi:10.1016/j.epsl.2015.07.042.

Cerney B, Carlson RL 1999. The effect of cracks on the seismic velocities of basalt from site 990, southeast Greenland margin. In: Proceedings of the Ocean Drilling Program, Scientific Results 163: 29-35.

Clarke BA, Burbank DW 2011. Quantifying bedrock-fracture patterns within the shallow subsurface: Implications for rock mass strength, bedrock landslides, and erodability. Journal of Geophysical Research 116; F04009. doi:10.1029/2011JF001987.

Chadwick OA, Gavenda RT, Kelly EF, Ziegler D, Olson CG, Elliott WC, Hendricks DM 2003. The impact of climate on the biogeochemical functioning of volcanic soils. Chem. Geol. 202; 193–221.

Dixon JL, Heimsath AM, Amundson R 2009. The critical role of climate and saprolite weathering in landscape evolution. Earth Surface Processes and Landforms 34(11); 1507-1521.

Dixon JL, Hartshorn AS, Heimsath AM, DiBiase RA, Whipple KX 2012. Chemical Weathering response to tectonic forcing: A soils perspective from the San Gabriel Mountains, California. Earth and Planetary Science Letters. 2012 Mar 15;323:40-9.

Duffaut, P 1981. Structural weaknesses in rocks and rock masses: Tentative classification and behaviour. In ISRM International Symposium. International Society for Rock Mechanics.

Duffy B, Campbell J, Finnemore M, Gomez C 2014. Defining fault avoidance zones and Associated geotechnical properties using MASW: a case study on the Springfield Fault, New Zealand. Engineering Geology 183; 216-229.

Ferrier KL, Kirchner JW 2008. Effects of physical erosion on chemical denudation rates: A numerical modeling study of soil-mantled hillslopes. Earth and Planetary Science Letters *272*(3); 591-599.

Foti S, Comina C, Boiero D, Socco LV 2009. Non-uniqueness in surface-wave inversion and consequences on seismic site response analyses. Soil Dynamics and Earthquake Engineering 29(6); 982-993.

Giambelluca TW, Chen Q, Frazier AG, Price JP, Chen YL, Chu PS, Eischeid JK, Delparte DM 2013. Online rainfall atlas of Hawai'i. Bulletin of the American Meteorological Society 94(3); 313-316.

Goodfellow BW, Chadwick OA, Hilley GE 2014. Depth and character of rock weathering across a basaltic hosted climosequence on Hawai ‘i. Earth Surface Processes and Landforms 39(3); 381-398.

Greenwood W, Zekkos D, Sahadewa A 2015. Spatial Variation of Shear Wave Velocity of Waste Materials from Surface Wave Measurements. Journal of Environmental and Engineering Geophysics *20*(4); 287-301.

Gupta AS, Rao KS 1998. Index properties of weathered rocks: inter-relationships and applicability. Bulletin of Engineering Geology and the Environment 57(2), 161-172.

Hachinohe S, Hiraki N, Suzuki T 1999. Rates of weathering and temporal changes in Strength of bedrock of marine terraces in Boso Peninsula, Japan. Engineering Geology 55; 29-43.

Han J, Gasparini NM, Johnson JP, Murphy BP 2014. Modeling the influence of rainfall gradients on discharge, bedrock erodibility, and river profile evolution, with application to the Big Island, Hawai'i. Journal of Geophysical Research: Earth Surface 119(6); 1418-1440.

Hoek E, Brown ET 1980. Empirical strength criterion for rock masses. Journal of Geotechnical and Geoenvironmental Engineering 106: ASCE 15715.

Hoek E 1994. Strength of rock and rock masses. ISRM News Journal 2(2); 4-16.

Hoek E, Brown ET 1997. Practical estimates of rock mass strength. International Journal of Rock Mechanics and Mining Sciences 34(8); 1165-1186.

Holbrook SW, Riebe CS, Elwaseif M, Hayes JL, Basler-Reeder K, Harry DL, MalazianA, Dosseto A, Hartsough PC, Hopmans JW 2014. Geophysical constraints on deep Weathering and water storage potential in the Southern Sierra Critical Zone Observatory. Earth Surface Processes Landforms 39; 366–380. doi: 10.1002/esp.3502.

Hayashi K, Suzuki H 2004. CMP cross-correlation analysis of multichannel surface wave data. Exploration Geophysics 35; 7-13.

Lamb MP, Howard AD, Dietrich WE, Perron JT 2007. Formation of amphitheater headed valleys by waterfall erosion after large-scale slumping on Hawai ‘i. Geological Society of America Bulletin 119(78); 805-822.

Larsen IJ, Almond PC, Eger A, Stone JO, Montgomery DR, Malcolm B 2014. Rapid soil production and weathering in the Southern Alps, New Zealand. Science *343*(6171); 637-640.

Lebedeva MI, Brantley SL 2013. Exploring geochemical controls on weathering and Erosion of convex hillslopes: beyond the empirical regolith production function. Earth Surface Processes and Landforms 38(15): 1793-807. doi:10.1002/esp.3424.

Marinos P, Hoek E 2001. Estimating the geotechnical properties of heterogeneous rock Masses such as flysch. Bulletin of engineering geology and the environment *60*(2); 85 92.

Marinos V 2010. New proposed GSI classification charts for weak or complex rock masses. Bull.Geol. Soc. Greece, Proc, of the 12th Int. Congress, Patras, May 2010.

McDougall I 1969. Potassium–argon ages of lavas from the Hawi and Pololu Volcanic Series, Kohala Volcano, Hawaii. Geol. Soc. Amer. Bull. 80; 2597–2600.

McDougall I, Swanson DA 1972. Potassium–argon ages of lavas from the Hawi and Pololu Volcanic Series, Kohala Volcano, Hawaii. Geol. Soc. Amer. Bull. 83; 3731–3738

Mohamed Z, Mohamed K, Gye Chun C 2008. Uniaxial compressive strength of composite rock material with respect to shale thickness ratio and moisture content. Electron J Geotech Eng *13*; 1-10.

Molnar P, Anderson RS, Anderson SP 2007. Tectonics, fracturing of rock, and erosion. Journal of Geophysical Research: Earth Surface *112*(F3).

Moon V, Jayawardane J 2004. Geomechanical and geochemical changes during early stages of weathering of Karamu Basalt, New Zealand. Engineering Geology 74; 57-72. doi:10.1016/j.enggeo.2004.02.002.

Murphy BP, Johnson JPL, Gaspirini NM, Sklar LS 2016. Chemical weathering as a mechanism for the climatic control of bedrock river incision. Nature 532; 223-227. doi:10.1038/nature17449

National Research Council 2001. Basic research opportunities in earth science. National Academy Press, Washington, D.C., 168 pp, ISBN: 0-309-56988-5.

Oki, DS, Gingerich, SB, and Whitehead, RL 1999. Hawaii *in* Ground Water Atlas of the United States, Segment 13, Alaska, Hawaii, Puerto Rico, and the US Virgin Islands: US Geological Survey Hydrologic Investigations Atlas 730-N, p N12-N22, N36.

OYO Corporation 2006. SeisImager/2D manual, Ver. 3.2. Available at ftp://geom.geometrics.com/pub/seismic/SeisImager/Intallation_CD/SeisImager2D_Manual/ (verified 2015)

Park CB, Miller RD, Xia J 1998. Imaging dispersion curves of surface waves on multi-channel record. Expanded Abstracts: 68th Annual International Meeting, Society of Exploration Geophysicists. 1377-1380.

Park CB, Miller RD, Xia J 1999. Multichannel analysis of surface waves. Geophysics 64(3); 800-808.

Parsekian AD, Singha K, Minsley BJ, Holbrook WS, Slater L 2015. Multiscale geophysical imaging of the critical zone. Rev. Geophys 53; 1-26. doi: 10.1002/2014RG000465.

Pelekis PC, Athanasopoulos GA 2011. An overview of surface wave methods and a Reliability study of a simplified inversion technique. Soil Dynamics and Earthquake Engineering 31(12); 1654-1668.

Porter SC 2005. Pleistocene snowlines and glaciation of the Hawaiian Islands. Quaternary International; 138-139: 118-128. doi:10.1016/j.quaint.2005.02.009.

Porder S, Hilley GE, Chadwick OA 2007. Chemical weathering, mass loss, and dust inputs across a climate by time matrix in the Hawaiian Islands. Earth and Planetary Science Letters 258(3); 414-427.

Rahardjo H, Aung KK, Leong EC, Rezaur RB 2004. Characteristics of residual soils in Singapore as formed by weathering. Engineering Geology 73(1): 157-69. doi:10.1016/j.enggeo.2004.01.002

Riebe, CS, Hahm, WJ, and Brantley, SL 2016. Controls on deep critical zone architecture: a historical review and four testable hypotheses. Earth Surface

Processes and Landforms; doi 10.1002/esp.4052.

Rempe DM, Dietrich WE 2014. A bottom-up control on fresh-bedrock topography under landscapes. Proceedings of the National Academy of Sciences 111(18): 6576-81. doi:10.1073/pnas.1404763111

Ritter D, Kochel CR, Miller JR 2011. Process Geomorphology, fifth edition.

Sarno A, Farah R, Hudyma N, Hiltunen DR 2010. Relationships between Compression Wave Velocity and Unconfined Compression Strength for Weathered Florida Limestone. In GeoFlorida 2010 Advances in Analysis, Modeling and Design ASCE; 950-959.

Selby MJ 1980. A rock mass strength classification for geomorphic purposes: with tests from Antarctica and New Zealand. Zeitschrift für Geomorphologie 24; 31-51.

Spengler SR, Garcia MO 1988. Geochemistry of the Hawi lavas, Kohala Volcano, Hawaii, Contributions to Mineralogy and Petrology 99; 90–104.

Stanchits S, Vinciguerra S, Dresen G 2006. Ultrasonic velocities, acoustic emission characteristics and crack damage of basalt and granite. Pure and Applied

Geophysics 163(5-6); 975-994.

St. Clair J, Moon S, Holbrook WS, Perron JT, Riebe CS, Martel SJ, Carr B, Harman C, Singha K, Richter DdeB 2015. Geophysical imaging reveals topographic stress control of bedrock weathering. Science 350 6260; 534-538. doi: 10.1126/science.aab2210.

Stokoe KH II, Wright SG, Bay JA, Roesset JM 1994. Characterization of geotechnical sites by SASW method. Geophysical Characterization of Sites, Woods, R. D., ed., International Science, New York; 15-26.

Stokoe KH, Santamarina JC 2000. Seismic-wave-based testing in geotechnical engineering. ISRM International Symposium. International Society for Rock Mechanics.

Tugrul A, Zarif IH 2000. The influence of weathering on the geological and geomechanical characteristics of a sandstone in Istanbul, Turkey. Environmental and Engineering Geoscience 6(4); 403-412.

Tziallas GP, Saroglou H, Tsiambaos G 2013. Determination of mechanical properties of flysch using laboratory methods. Engineering Geology 166: 81-89.

West AJ, Galy A, Bickle M 2005. Tectonic and climatic controls on silicate weathering. Earth and Planetary Science Letters 235(1); 211-228.

Wolfe EW, Morris J 1996. Geologic map of the Island of Hawaii No. 2524-A.

Wong IG, Stokoe KH, Cox BR, Yuan J, Knudsen KL, Terra F, Okubo P, Lin YC 2011. Shear-wave velocity characterization of the USGS Hawaiian strong-motion network on the island of Hawaii and development of an NEHRP site-class map. Bulletin of the Seismological Society of America 101(5); 2252-2269.

Xia J, Miller RD, Park CB, Ivanov J 2000. Construction of 2-D vertical shear-wave velocity field by the multichannel analysis of surface waves technique. Proceedings of the Symposium on the Application of Geophysics to Engineering and Environmental Problems, Arlington, VA, 20-24 Feb. 2000, 1197-1206.

Xia J, Miller RD, Park CB, Tian G 2003. Inversion of high frequency surface waves with Fundamental and higher modes. Journal of Applied Geophysics 52; 45-57.

Yoon S, Rix JG 2009. Near-field effects on array-based surface wave methods with active sources. Journal of Geotechnical and Geoenvironmental Engineering 135(3);

399-406.

Zekkos D, Cohen-Waeber J, Medley E, Jesionek K 2008. Characterization of weak rock mass and geoengineering analyses for a canyon landfill in northern California. Paper #6.05a, 6th International Conference on Case Histories in Geotechnical Engineering, Arlington, VA, August 11-16, 2007 (in proceedings cd).

FIGURE CAPTIONS

Figure 1. Geologic map of Kohala district of Hawai'i with seismic survey locations (dots). Mean annual precipitation (MAP) in mm/yr is derived from Giambelluca et al. (2013).

Figure 2. P-wave and S-wave velocity models for dry sites (MAP 500-600 mm/yr). Multiple profiles at a single site display results from different geophone spacings and dashed lines represent survey overlap. Smaller geophone spacing resolves greater detail near the surface of the profile (right panels).

Figure 3. P-wave velocity models for wet sites (MAP 1000-3000 mm/yr). Sites with multiple profiles vary in geophone spacings and dashed lines represent survey overlap. Shorter geophone spacing resolves greater detail near the surface of the profile.

Figure 4. S-wave velocity models for two wet sites. The low-velocity horizon at ~ 4 m depth corresponds to a soft, weathered horizon observed in the sea cliff (top right) adjacent to the seismic survey.

Figure 5. P-wave velocity model of Road Cut East site compared to a weathering profile interpretation and Silver Schmidt Hammer rebound measurements. A) Photograph of section exposure from Road Cut East seismic site (Figures 1 and 2), which was collected parallel to and 5 m back from the photographed road cut. B) Weathering interpretation and descriptions of Goodfellow et al. (2014) for the same road cut. Numbers in white indicate Silver Schmidt rebound hammer Q values (average, n=10) measured on the outcrop. C) Select portion of velocity profile from Road Cut East, 1 meter line (Figure 2), which overlaps road cut section. Black lines represent interpreted soil, saprolite+weathered rock, and vesicular/highly fractured, unaltered rock layers interpreted from the road cut section.

Figure 6. Averaged P and S wave velocity as a function of depth (thick and thin lines respectively). Dry sites (500-600 mm/yr) MAP show rapid increases in velocity with depth. These profiles reach unweathered basalt velocities (Wong et al., 2011) at ~ 4-10 m depth. Sites with 1000 mm/yr MAP and greater display more gradual increase in velocity with depth and do not vary significantly with precipitation. The average velocity-depth gradient is in agreement with previous S-wave profiles in Kohala on Pololu units (Wong et al., 2011). Average velocities of these high precipitation sites approach our interpreted "unaltered basalt" values within the maximum depth of investigation (15-25 m) but do not reach the "unweathered basalt" values proposed by Wong et al., 2011.

Figure 7. Hypothetical slip-surfaces for slopes with two different strength profiles. The back-calculated shear strength will depend on the weighted average of material strength, τ, along the slip surface. Thus the relative differences in bulk strength between the two profiles will depend on the relative differences in τ between the different layers, and the surface area of each layer along the failure plane. In Kohala, we suggest that the observed horizontal layers of slightly weathered to unweathered rock in the near-surface profile may contribute significantly to the strength of steep hillslopes.

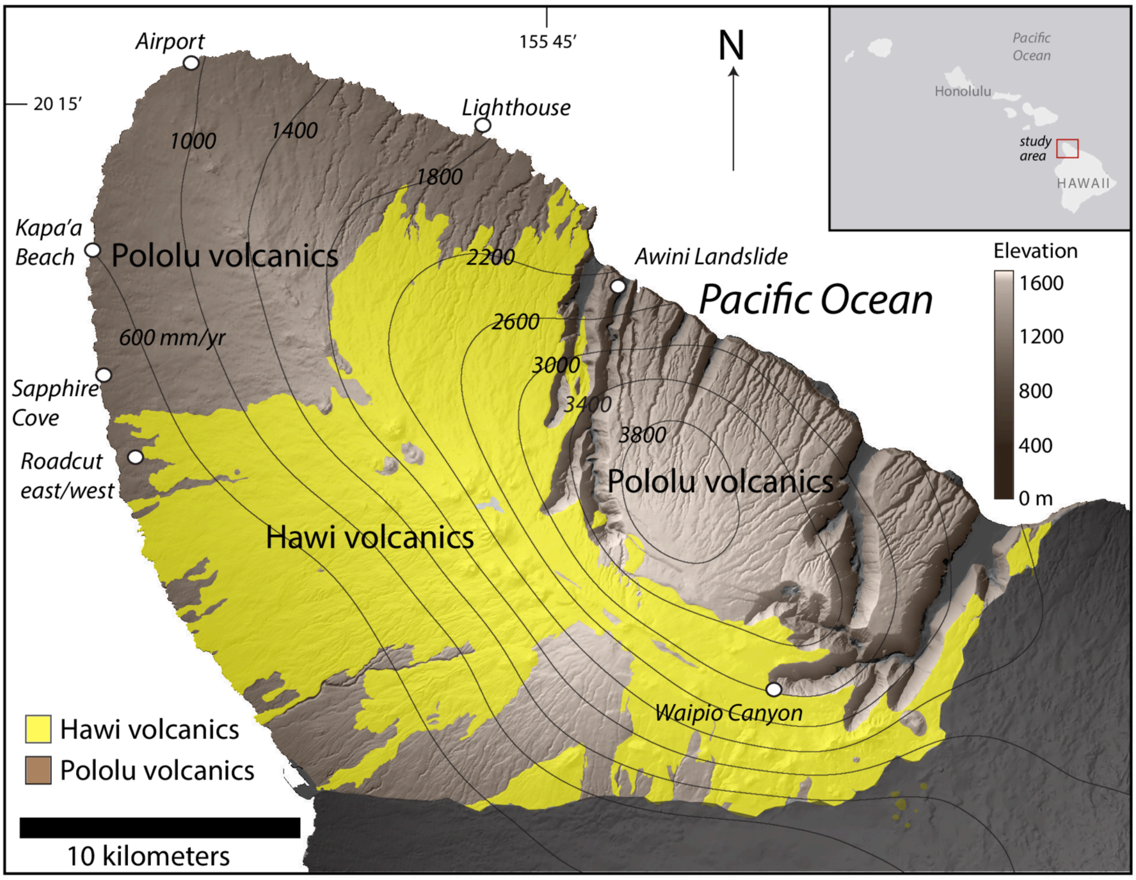

Figure 1

esp_4290_f1.ai

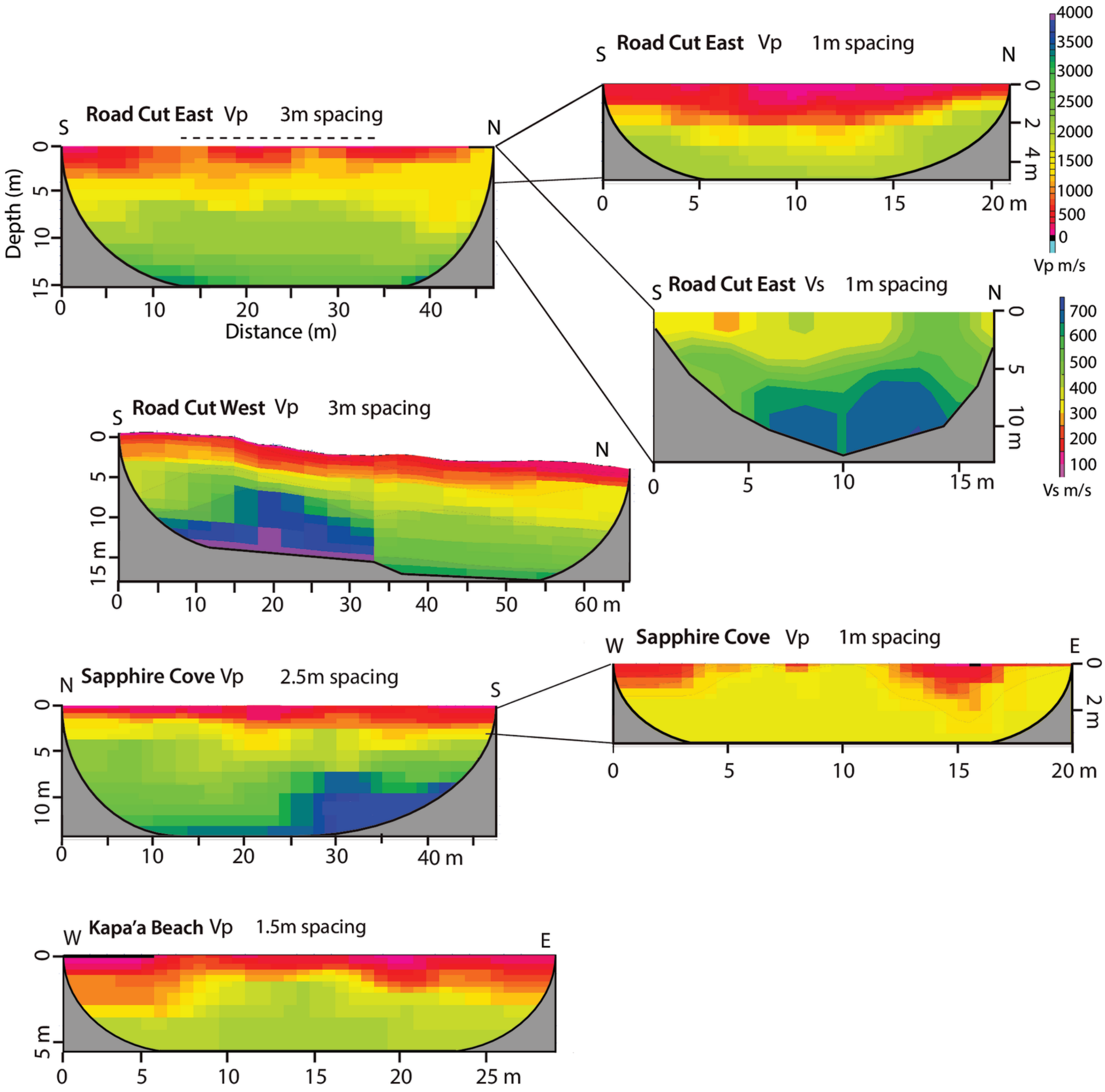

Figure 2

esp_4290_f2.ai

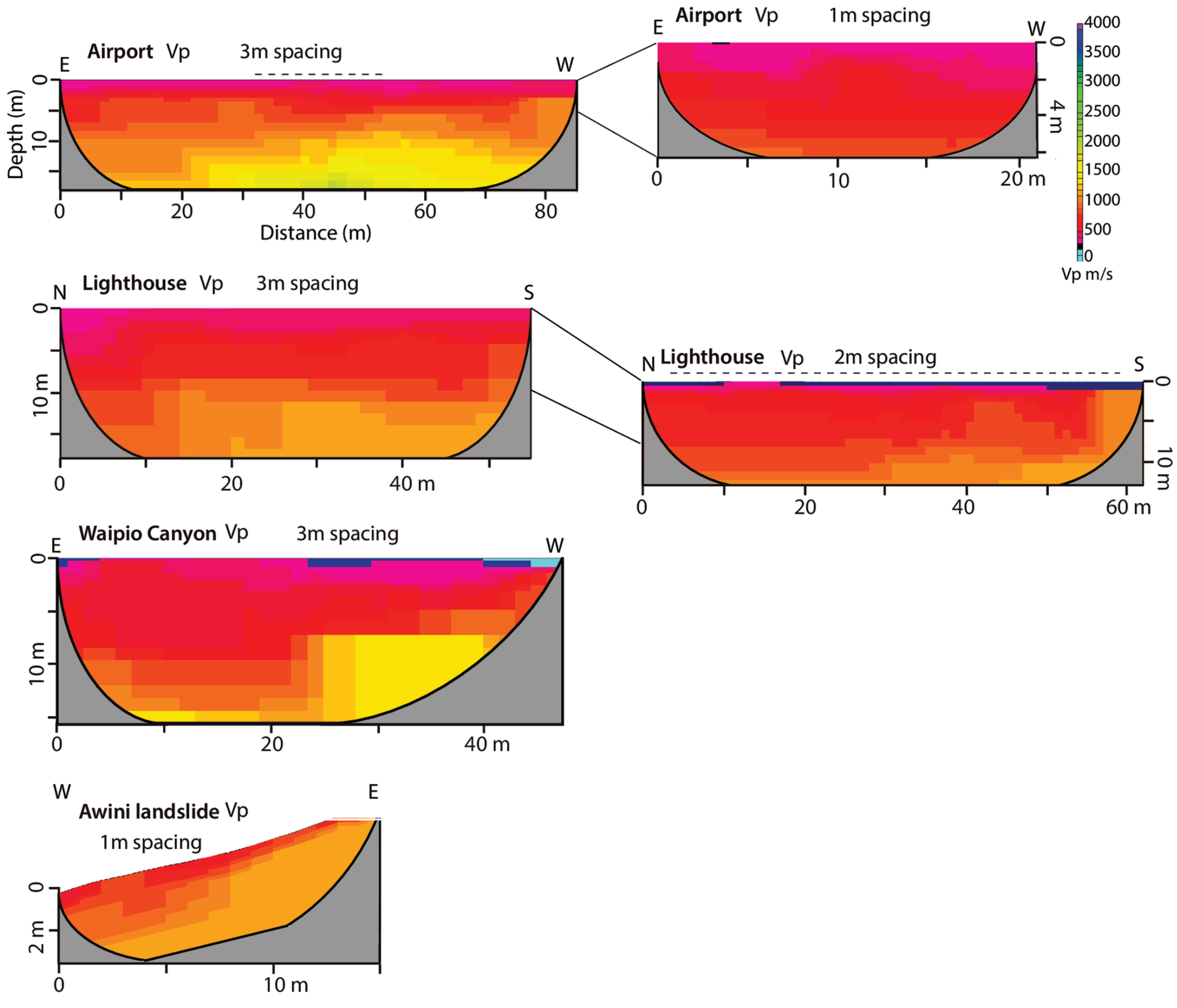

Figure 3

esp_4290_f3.ai

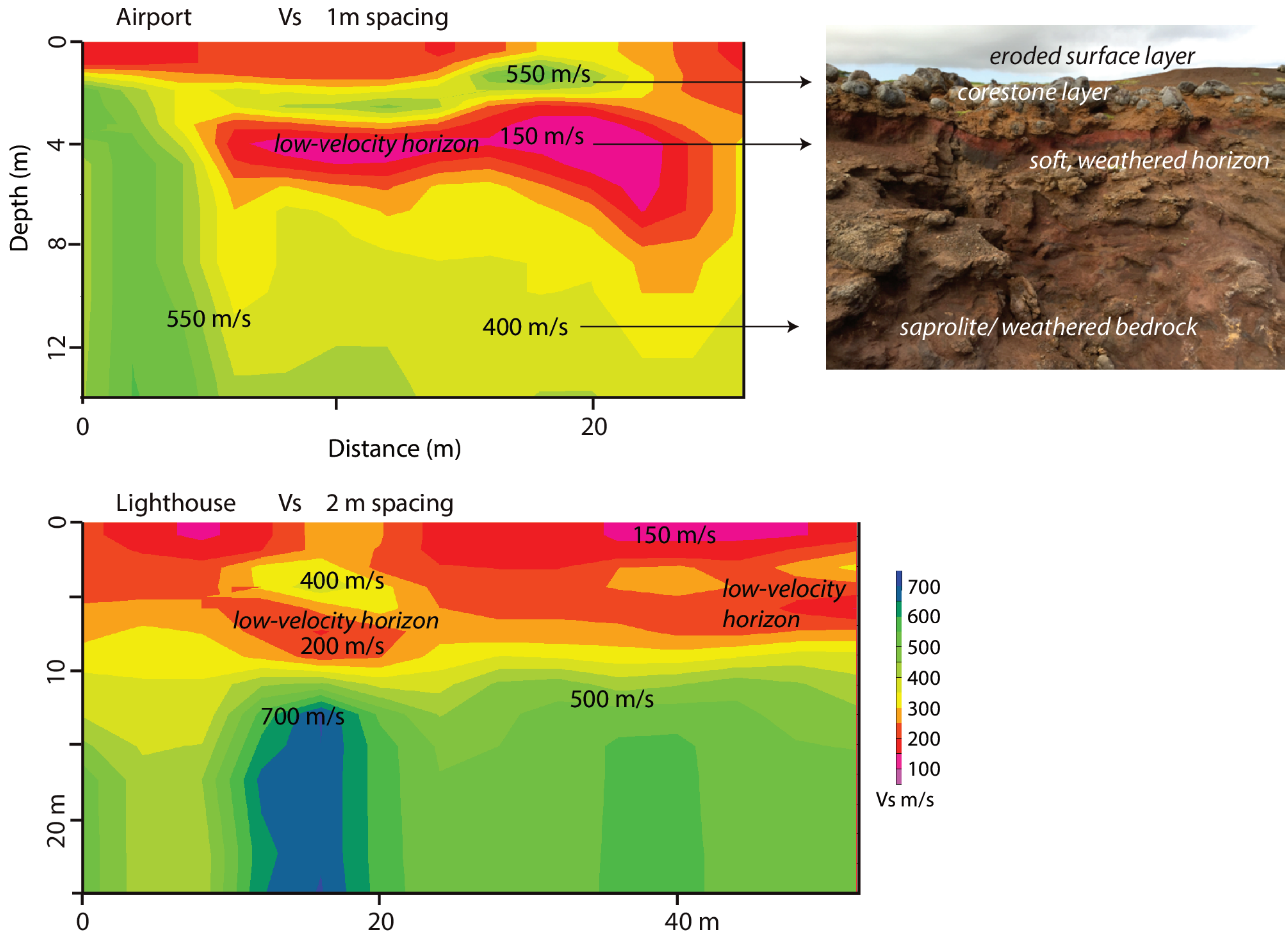

Figure 4

esp_4290_f4.ai

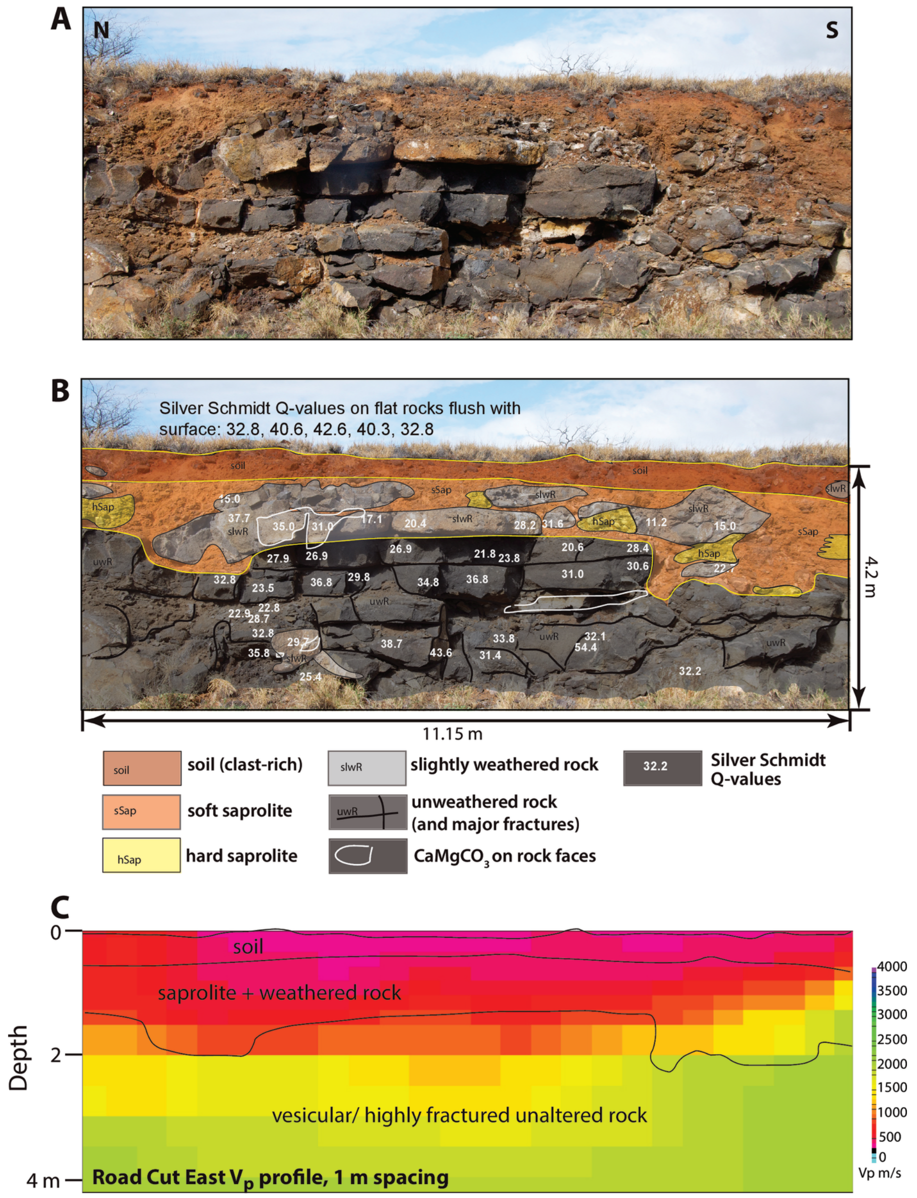

Figure 5

esp_4290_f5.ai

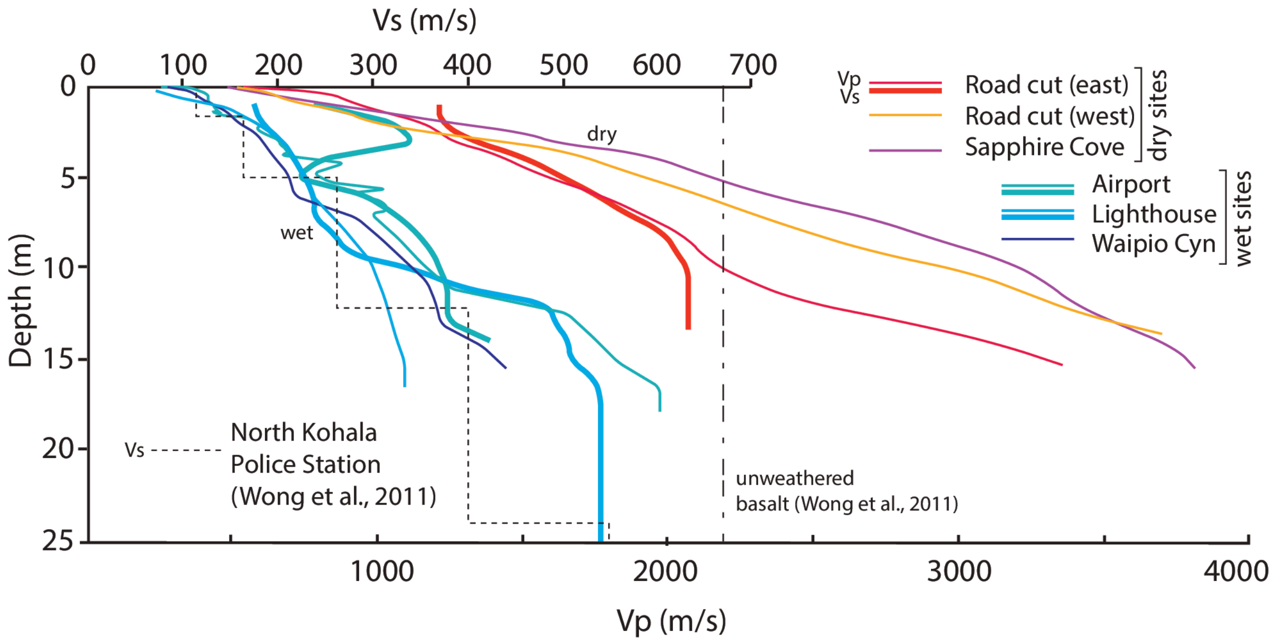

Figure 6

esp_4290_f6.ai

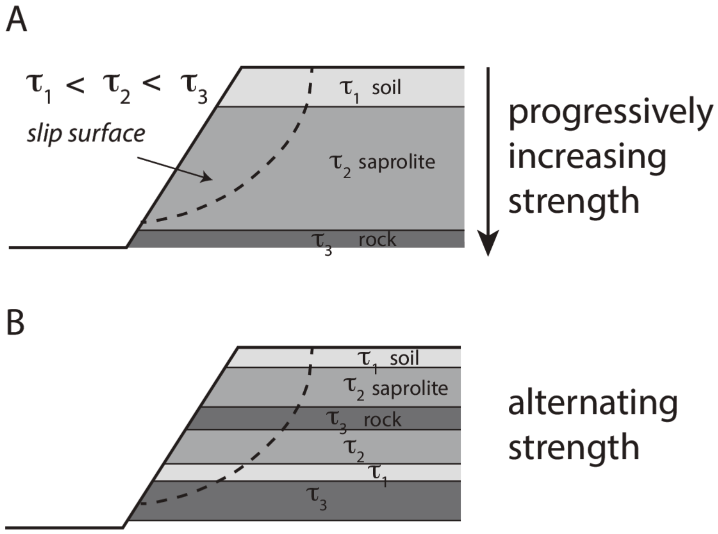

Figure 7

esp_4290_f7.ai